A four-year record of $U^{K'}_{37}$- and TEX_{86}-derived sea surface temperature estimates from sinking particles in the filamentous upwelling region off Cape Blanc, Mauritania

Gesine Mollenhauer[a,b*], Andreas Basse[a,b], Jung-Hyun Kim[c], Jaap S. Sinninghe Damsté[c], Gerhard Fischer[b]

[a]*Alfred Wegener Institute, Helmholtz Center for Polar and Marine Sciences, D-27570 Bremerhaven, Germany*
[b] *Department of Geosciences and MARUM center for Marine Environmental Sciences, University of Bremen, D-28334 Bremen, Germany*
[c]*NIOZ Royal Netherlands Institute for Sea Research, Department of Marine Organic Biogeochemistry, NL-1790 AB Den Burg, The Netherlands*

*corresponding author; gesine.mollenhauer@awi.de

Abstract

Lipid biomarker records from sinking particles collected by sediment traps can be used to study the seasonality of biomarker production as well as processes of particle formation and settling, ultimately leading to the preservation of the biomarkers in sediments. Here we present records of the biomarker indices $U^{K'}_{37}$ based on alkenones and TEX_{86} based on isoprenoid glycerol dialkyl glycerol tetraethers (GDGTs), both used for the reconstruction of sea surface temperatures (SST). These records were obtained from sinking particles collected using a sediment trap moored in the filamentous upwelling zone off Cape Blanc, Mauritania, at approximately 1300 water depth during a four-year time interval between 2003 and 2007, and supplemented by $U^{K'}_{37}$ and TEX_{86} determined on suspended particulate matter collected from surface waters in the study area. Mass and lipid fluxes are highest during peak upwelling periods between October and June. The alkenone and GDGT records both display pronounced seasonal variability. Sinking velocities calculated from the time lag between measured SST maxima and minima and corresponding index maxima and minima in the trap samples are higher for particles containing alkenones (14-59 m d^{-1}) than for GDGTs (9-17 m d^{-1}). It is suggested that GDGTs are predominantly exported from shallow waters by incorporation in opal-rich particles. SST estimates based on the $U^{K'}_{37}$ index correspond to the amplitude observed fluctuations in SST during the study period. Temperature estimates based on TEX_{86} show smaller seasonal amplitudes, which can be explained by either predominant production of GDGTs during the warm season, or a contribution of GDGTs exported from deep waters, which are in this region known to carry GDGTs in a distribution that translates to a high TEX_{86} signal.

Key words: Sinking particles, particle flux, $U^{K'}_{37}$, TEX_{86}, coastal upwelling system

1. Introduction

Reconstruction of sea surface temperature (SST) based on geochemical proxies has for the past decades been one of the central themes in paleoclimate research. Among the geochemical proxies, two relatively well-established proxies rely on the abundance ratio of specific organic biomarkers in the sediments. The degree of unsaturation of C_{37} alkenones produced predominantly by specific Prymnesiophyceae, namely *Emiliania huxleyi* and *Gephyrocapsa oceanica*, commonly expressed using the $U^{K'}_{37}$ index (Prahl and Wakeham, 1987), shows a linear correlation with SST and has supported important insights into the climate system (e.g., Kienast *et al.*, 2006; Lamy *et al.*, 2004; Rühlemann *et al.*, 1999). The tetraether index of glycerol dialkyl glycerol tetraethers (GDGTs) with 86 carbon atoms (TEX_{86}) (Schouten *et al.*, 2002)) is based on the distribution of membrane lipids of marine planktonic Thaumarchaeota, formerly known as Group I Crenarchaeota (e.g., Brochier-Armanet *et al.*, 2008; Spang *et al.*, 2010). It is increasingly applied in paleoclimatic studies, often in areas with sediments that lack sufficient quantities of alkenones and in studies of pre-Pleistocene time periods (e.g., Kim *et al.*, 2012, Etourneau *et al.*, 2013; Shevenell *et al.*, 2011; Sluijs *et al.*, 2006).

Global core-top calibrations of the SST proxies $U^{K'}_{37}$ (Conte *et al.*, 2006; Müller *et al.*, 1998) and TEX_{86} (Kim *et al.*, 2010) allow the general assumption that the indices correlate with annual mean SST. However, as the source organisms are known or inferred to occur seasonally (e.g., Brassell *et al.*, 1986; Conte *et al.*, 2006; Herfort *et al.*, 2006; Leider *et al.*, 2010; Martínez-Garcia *et al.*, 2009; Schneider *et al.*, 2010; Sikes *et al.*, 2002; Wuchter *et al.*, 2006), it is conceivable that the proxy signals should rather correspond to the respective season of maximum production, which will be site dependent. A further complication for the interpretation of TEX_{86} stems from several recent studies that have suggested that export of GDGTs may occur primarily from subsurface waters between 40 m and 150 m rather than from surface waters (Chen *et al.*, 2014; Huguet *et al.*, 2007; Lee *et al.*, 2008; Lopes dos Santos *et al.*, 2010). These studies based their interpretation on a better agreement of reconstructed temperatures using published calibrations of TEX_{86} (hereafter referred to as TEX_{86}-temperatures) with temperatures observed at deeper water depths than with SST. Consequently, when deviations between SST reconstructions based on $U^{K'}_{37}$ and TEX_{86} are encountered, they are often attributed to a potential difference in seasonality (e.g., Castañeda *et al.*, 2010;

Huguet *et al.*, 2006b; Lopes dos Santos *et al.*, 2013), or to a difference in depth habitat (e.g., Kim *et al.*, 2012; Lopes dos Santos *et al.*, 2010; Rommerskirchen *et al.*, 2011). However, recent studies on suspended particulate matter (SPM) collected from waters deeper than approximately 200 m have revealed that Thaumarchaeota living in these water depths likely produce GDGTs carrying a TEX_{86}-temperature different from the temperature relationship observed for surface sediment and SST, resulting in unrealistically high temperature estimates (Basse *et al.*, 2014; Schouten *et al.*, 2012).

In order to be preserved in sediments, the lipids synthesized in near-surface waters need to be exported to the deep ocean. There is evidence for the lipids to be incorporated in zooplankton faecal pellets (Grice *et al.*, 1998; Huguet *et al.*, 2006a). Alternatively to being grazed on by zooplankton, intact cells of the precursor organisms might become entrained in marine snow particles. The rate at which particles carrying lipids sink to the deep ocean is an important variable in determining the efficiency of export. Degradation rates strongly depend on packaging and on sinking velocities (Iversen and Ploug, 2010). It has been observed that the type of ballasting material in marine snow aggregates (e.g, carbonate or opal) determines the sinking velocity, where carbonate-ballasted aggregates sink up to 2.5 times faster than opal-ballasted aggregates (Iversen and Ploug, 2010). For GDGTs, in particular, understanding the process of export is important, as the small (<1 μm) and neutrally buoyant Thaumarchaeota cannot sink by themselves. Thaumarchaeota are distributed throughout the entire water column (Karner *et al.*, 2001), although cell numbers decrease with increasing depth. Since TEX_{86} is globally most highly correlated with SST, an efficient export of Thaumarchaeotal GDGTs from surface waters must exist. It has been proposed that GDGTs from surface waters in the Black Sea are preferentially exported due to grazing and packaging into sinking particles, which occurs primarily in shallow water depths (Wakeham *et al.*, 2003). This was supported by the fact that the distribution of GDGTs in the deep waters was completely different from that in the surface sediments. However, little is still known about the exact process of export of these lipids. All in all, it appears that there is still an incomplete understanding of seasonality of the source organisms in the World's ocean, how the lipids produced by the planktonic organisms are exported to the sediments, and which processes govern their export.

Samples collected by sediment traps are excellently suited for the study of organic biomarkers on their way to the sediment (Müller and Fischer, 2001). They allow a direct

comparison of the signals recorded with the actual SST prevailing at the time of production and, thus, assessment of whether or not the exported material does reflect sea-surface or sub-surface conditions. In a recent review study, Rosell-Melé and Prahl (2013) examined the influence of seasonality of alkenone production on alkenone flux to the sediment and the integrated sedimentary signal by using sediment trap data from all over the world. For their study, they used published alkenone flux data from sediment trap time series from 34 locations. Large regions of the world remain under-represented in this compilation, including much of the Atlantic Ocean and most of the Southern Hemisphere. Only about one third of those records cover more than one year.

In contrast, only six marine sediment-trap time series have been published for TEX_{86} (Fallet *et al.*, 2011; Huguet *et al.*, 2007; McClymont *et al.*, 2012; Turich *et al.*, 2013; Wuchter *et al.*, 2006; Yamamoto *et al.*, 2012), and only some of these also include alkenone data for comparison. Wuchter et al. (2006) observed a strongly seasonally varying GDGT flux and TEX_{86}-temperatures corresponding to SST in a shallow trap (500 m water depth), and more seasonally averaged signals in deeper traps. Weak seasonal variations and a better agreement of TEX_{86}-temperatures with mean annual temperatures were also observed in other sediment trap studies, in particular in deeper traps (Fallet *et al.*, 2011; McClymont *et al.*, 2012; Turich *et al.*, 2013; Yamamoto *et al.*, 2012).

Here we present records of sinking particles collected using a sediment trap moored at a eutrophic location within the Cape Blanc filament at approximately 1300 m water depth off Cape Blanc, Mauretania, spanning a four-year period from 2003 to 2007. Our data set includes mass fluxes, fluxes of alkenones and GDGTs as well as $U^{K'}_{37}$ and TEX_{86}. We observe pronounced seasonal variations in all records. Besides, we compare $U^{K'}_{37}$ and TEX_{86} signals of SPM from surface waters with in–situ temperature at the time of collection. We discuss the implications for seasonal occurrence, export mechanisms, calibrations, and consequences for the use of the proxies in sediments.

2. Study Area

The site of the sediment trap mooring array $CB_{eutrophic}$ (CBeu) is located off Mauritania (Northwest Africa) within the Canary Current (CC) System, which is one of the four major Eastern Boundary Upwelling Ecosystems (EBUEs) (Fig. 1). EBUEs are important ecosystems characterized by high primary production (Carr *et al.*, 2006) and

elevated organic carbon export to the deep ocean. Despite their relatively small size, they contribute roughly 10% to the total global marine primary production (Behrenfeld and Falkowski, 1997). As for other EBUEs, the Canary Current System has several well-defined subzones/biomes (Fréon *et al.*, 2009). The area offshore Cape Blanc between 19 and 24°N (north of the Cape Verde Frontal Zone, CVFZ) is defined as a northern Inter-Gyre region with weaker seasonality and more persistent upwelling but with peaks in winter to spring and fall (e.g., Lathuilière *et al.*, 2008; Mittelstaedt, 1991). The trade winds blow rather continuously all year long, being intensified sometime around springtime (e.g., Meunier *et al.*, 2012). This results in intensified upwelling between approximately January and June. In the Mauritanian upwelling, the biological response, i.e. higher chlorophyll standing stocks to alongshore wind forcing appears to be almost immediate (Pradhan *et al.*, 2006). At Cape Blanc, a tongue of cold water spreads several hundreds of kilometres offshore, forming the 'giant Cape Blanc filament' (Van Camp *et al.*, 1991), the largest filament within all EBUEs.

Lathuiliere et al. (2008) provide a comprehensive overview of the ocean circulation of the study area. The cold and nutrient-rich southward flowing CC departs from the coast and later forms the North Equatorial Current (NEC) (Fig. 1). During summer and fall, a poleward flow along the Mauritanian coast, the Mauritanian Current (MC) originating from the North Equatorial Counter Current (NECC), moves to about 20°N (Mittelstaedt, 1991) bringing warmer water masses from tropical areas into the study site. There, a NE-SW oriented salinity front in the subsurface waters, the CVFZ, is found (Zenk *et al.*, 1991) (Fig. 1), separating the salty and nutrient-poor North Atlantic Central Water (NACW) from the nutrient-richer and cooler South Atlantic Central Water (SACW). Both water masses may be upwelled and mixed laterally and frontal eddies develop at the CVFZ (Meunier *et al.*, 2012). South of the CVFZ, a recirculation gyre between 10 and 19°N is found, with stronger seasonality and a large offshore extension of the high-chlorophyll area from February to May (Lathuilière *et al.*, 2008).

3. Material and Methods

3.1 Sample material

The sediment trap CBeu was moored at a eutrophic site within the filamentous zone of the Cape Blanc upwelling cell at a water depth of approximately 1300 m (Fig. 1). The water depth at this site is approximately 2690 m. We used samples collected during

four deployment periods between June 2003 and March 2007. Exact sampling periods and mooring locations are summarized in Table 1. The trap consisted of a Kiel-type large-aperture sediment trap with an opening of 0.5 m^2 covered with a honeycomb baffle to reduce turbulence. The traps were equipped with 20 cups, which were poisoned using $HgCl_2$ before and after deployment by addition of 1 mL of a saturated $HgCl_2$ solution in distilled water at 20°C per 100 mL. Pure NaCl was used to increase the density in the cups (40‰) prior to the deployments. Large swimmers were removed manually, and other swimmers were removed by filtering carefully through a 1 mm sieve. Thus all fluxes here refer to the size fraction of <1mm. In almost all cases, the fraction of particles >1mm was negligible. Samples were wet-split in the home laboratory using a rotating McLane wet splitter system and subsequently freeze-dried (for a detailed description of the methods see Fischer and Wefer 1991).

Surface sediment sample GeoB13612-3 was taken at the trap mooring location (20°45.1'N, 18°42.04'W, 2691 m water depth) using a multi-corer during R/V Maria Sibylla Merian (MSM) cruise 11-2 (Bickert *et al.*, 2011). One subcore of the multi-core was sectioned on-board in 1 cm slices and stored in pre-combusted glass jars at -20°C until further processing in the laboratory. Here we analysed only the uppermost 0-1 cm.

Suspended particulate material (SPM) was collected in March and April 2009 during cruising and station work of cruise MSM 11-2 and in February and March 2010 during RV Poseidon cruise POS 396 (Fischer and participants, 2011) by filtering sea-water taken from the ship's sea-water inlet located at approximately 5 m below sea-level. Approximately 45-300 L of seawater were filtered onto pre-combusted 142 mm diameter GF/F filters, and SST at the time and location of sampling were recorded (see Table 2 for exact locations and volumes). Filters were wrapped in pre-combusted Aluminium-foil and stored at -20°C until further processing in the home laboratories. The sampling periods correspond to the early to peak upwelling season in the study region. SSTs during sampling were recorded by the ships' thermometer.

3.2 Laboratory methods

Sediment trap samples were analyzed according to Fischer and Wefer (1991) using 1/5 wet splits of the fraction <1mm. Samples were freeze-dried, and the homogenized samples were weighed for total mass and analysed for organic carbon, total nitrogen, carbonate and biogenic opal. Total organic carbon (TOC), total nitrogen (TN) and calcium carbonate were measured by combustion with a CHN analyzer

(HERAEUS). TOC was measured after removal of carbonate with 2 N HCl. Overall analytical precision based on internal lab standards was better than 0.1% (±1σ). Carbonate was determined by subtracting TOC from total carbon, the latter being measured by combustion without pre-treatment with 2N HCl. Biogenic opal was determined with a sequential NaOH-leaching technique (Müller and Schneider, 1993). The precision of the overall method based on replicate analyses is mostly between ±0.2 and ±0.4%, depending on the material analyzed. For a detailed table of standard deviations for various samples we refer to Müller and Schneider (1993). Lithogenic fluxes were calculated from total mass flux by subtracting the flux of carbonate, opal and two times the flux of TOC to approximate organic matter.

Freeze-dried sediment trap and surface sediment samples were homogenized using an agate mortar and pestle. Filters were oven dried at 36°C for 24 h. After addition of known amounts of squalane, C_{19} ketone as internal standard, filters, 0.04 to 0.1 g of homogenized sediment trap samples and 3 g of surface sediment were extracted according to the protocol described by Müller et al. (1998). Briefly, total lipid extracts (TLEs) were obtained using ultrasonic disruptor probes and 25 mL of successively less polar (methanol, methanol:dichloromethane 1:1 v:v, dichloromethane) solvents. Extracts were combined and washed with 50mL de-ionized water to remove salts. The organic solvent fraction was recovered, dried with anhydrous sodium sulphate and reduced to dryness using rotary evaporation. TLEs were saponified in a solution of potassium hydroxide in methanol and water (9:1 v:v) at 80°C for two hours. Neutral lipids recovered in hexane were subsequently fractionated into three polarity fractions using Bond-Elut silica gel cartridges. Fractions 1 to 3 were eluted in 2 mL each of hexane, hexane:dichloromethane 1:2 v:v, and methanol, respectively.

Fractions 2 were dried, re-dissolved in 25 µL of dichloromethane:methanol (1:1 v:v) and analysed for alkenone concentrations and relative abundances using an Agilent 5890 gas chromatograph equipped with a DB5-MS capillary column and a flame ionization detector. Alkenones were identified based on relative retention time and comparison with a laboratory-internal standard sediment, and the $U_{37}^{K'}$ index was calculated using peak areas of the di- and tri-unsaturated C_{37} alkenones, i.e. $C_{37:3}$ and $C_{37:2}$ alkenones according to Prahl and Wakeham (1987).

$$U_{37}^{K'} = \frac{[C37:2]}{[C37:2] + [C37:3]} \quad (1)$$

248

249 $U^{K'}_{37}$ values were converted to temperature estimates using the temperature

250 calibrations of Conte et al. (2006).

251

252 $T\ (°C) = -0.957 + 54.293 \times (U^{K'}_{37}) - 52.894 \times (U^{K'}_{37})^2 + 28.321 \times (U^{K'}_{37})^3$ (for SPM)(2)

253

254 annual mean SST (AnnO) (°C) $= 29.876 \times (U^{K'}_{37}) - 1.334$ (for core-top sediments)

255 (3)

256

257 Concentrations were determined relative to the internal standard C_{19} ketone and

258 assuming the same relative response factor for C_{37} alkenones as for C_{36} *n*-alkane

259 determined in external standard runs. Analytical precision based on repeated analyses

260 of the lab-internal sediment standard is +/-0.01 units of the $U^{K'}_{37}$ index and 10% for

261 alkenone concentrations.

262 Fractions 3 containing the polar lipids were weighed in pre-weighed glass vial

263 inserts, re-dissolved in hexane:isopropanol (99:1 v:v) to obtain a concentration of 2

264 mg/mL and filtered through 4 mm diameter 0.45 μm pore size PTFE syringe filters as

265 described by Hopmans et al. (2000). The filtered fractions were analysed for GDGTs

266 using high performance liquid chromatography/atmospheric pressure chemical

267 ionization mass spectrometry (HPLC/APCI-MS) according to the protocol described by

268 Schouten et al. (2007). Trap series CBeu-2o to CBeu-4o were analysed in Bremen using

269 an Agilent 1200 series HPLC coupled with an Agilent 6120 MSD using single ion

270 monitoring mode. Details of the method are described in Leider et al. (2010). Peak areas

271 of masses (M/Z) 1302, 1300, 1298, 1296, 1292 for isoprenoidal GDGTs and 1050, 1036

272 and 1022 for branched GDGTs were determined. TEX_{86} and BIT index were calculated

273 according to Schouten et al. (2002) and Hopmans et al. (2004), respectively.

274

275 $$TEX_{86} = \frac{[GDGT-2]+[GDGT-3]+[Cren']}{[GDGT-1]+[GDGT-2]+[GDGT-3]+[Cren']} \quad (4)$$

276

where the numbers refer to the numbers of rings in the isoprenoid GDGTs, respectively, and Cren' is the regio-isomer of crenarchaeol.

$$\text{BIT index} = \frac{[\text{Ia}]+[\text{IIa}]+[\text{IIIa}]}{[\text{Ia}]+[\text{IIa}]+[\text{IIIa}]+[\text{IV}]} \quad (5)$$

Here, the roman numerals refer to the branched GDGTs with m/z of their hydrogenated molecular ions of 1022 (Ia), 1036 (IIa), and 1050 (IIIa), while (IV) is crenarchaeol.

TEX_{86} values were converted to temperatures using the global core-top calibrations for 0 m water depth (eq. 6; Kim et al., 2010) and for 0-200 m water depth (eq. 7; Kim et al., 2012):

$$T\ (°C) = 68.4 \times \log(TEX_{86}) + 38.6 \quad (6)$$

$$T\ (°C) = 54.7 \times \log(TEX_{86}) + 30.7 \quad (7)$$

Furthermore, a temperature calibration for TEX_{86} obtained on SPM from <100 m water depth (Schouten et al., 2013) was used:

$$T\ (°C) = 59.6 \times \log(TEX_{86}) + 32.0 \quad (8)$$

Concentrations of GDGTs could not be determined due to the lack of an internal standard at the time of analysis. However, the relative variability of GDGT concentrations were determined using the peak areas, injection volume and sediment mass. GDGT concentrations therefore can only be expressed in arbitrary units, but the relative changes within a trap series remain valid. Analytical precision based on

299 repeated analyses of the lab-internal sediment standard is +/-0.01 units of the TEX_{86}
300 index.
301 GDGTs of trap series CBeu-1o and a set of five selected samples from the later
302 series were analysed at the Royal Netherlands Institute for Sea Research using an
303 Agilent 1100 series HPLC/APCI-MS instrument as described by Schouten et al. (2007).
304 The results of the selected repeat analyses are identical within error with the
305 measurements in Bremen, as was to be expected according to the inter-laboratory
306 comparison experiment (Schouten *et al.*, 2013a).
307
308 **4. Results**
309
310 *4.1 Alkenone and GDGT composition of suspended particulate matter*
311 The $U_{37}^{K'}$ values obtained for 37 samples of SPM collected on filters from the ships'
312 sea water inlets during cruises MSM11-2 and POS396 range from 0.31 to 0.86, and TEX_{86}
313 values vary between 0.47 and 0.71 (Table 2). The $U_{37}^{K'}$ displays a relationship with
314 measured SST that is in agreement with the global relationship Conte et al. (2006)
315 reported for SPM (Figure 2a). Three samples (filters 21, 32, and 37; Table 2) have a
316 lower $U_{37}^{K'}$ value than expected for the respective observed SST when compared with
317 the published data set. The TEX_{86} values are also within the range of observed SPM
318 TEX_{86} as compiled by Schouten et al. (2013b) (Figure 2b). However, our data cluster
319 below the regression line indicating that the proposed calibration would yield lower
320 TEX_{86}-temperatures than measured.
321 When compared with the core-top sediment data set of Conte et al. (2006), the
322 SPM $U_{37}^{K'}$ values are lower at a given SST than those in observed in sediments,
323 particularly around 20°C, while those of our SPM $U_{37}^{K'}$ from the warmest regions do not
324 show such a mismatch (Figure 2c). In contrast, the TEX_{86} values of SPM at the given SST
325 are within the range observed in the global core-top dataset used for the most recent
326 calibration (Figure 2d) (Kim *et al.*, 2010).
327
328 *4.2 Mass, alkenone and GDGT fluxes*
329 Mass fluxes to the sediment trap range between approximately 5 and 1500 mg m^{-2}
330 d^{-1} (mean ± std dev.: 340±290 mg m^{-2} d^{-1}) and display a distinct seasonal cycle (Figure
331 3f). Maxima of 0.6 to 1.5 g m^{-2} d^{-1} are reached during the winter to spring

(December/January to April/May) upwelling season, while the minima generally occur in late summer and autumn. An inter-annual variability is also evident, resulting in strongly variable absolute flux values both during the high and low flux seasons. In particular, hardly any material reached the trap during the low flux seasons in 2004 and 2006, while in 2005 even a secondary flux maximum was observed in autumn. Besides, the season of highest flux varies between February to May in 2004, December to March in 2005, and March to April in 2006. Summer (June to August) maxima occur in 2003 and 2006.

Fluxes of opal and total organic carbon (TOC) co-vary seasonally with the total fluxes and range between 0.5 - 290 mg m^{-2} d^{-1} and 0.8 - 97 mg m^{-2} d^{-1}, respectively (Figure 3f). Both these fluxes are strongly correlated with total flux (r^2=0.83 for opal and r^2=0.90 for TOC; Figure 4 a, b). Likewise, carbonate and lithogenic fluxes display seasonal variations (1.4 – 920 mg m^{-2} d^{-1} and 0 - 540 mg m^{-2} d^{-1}, respectively) and are correlated with mass flux, but their correlation coefficients (r^2=0.75 for carbonate and r^2=0.71 for lithogenic matter; not shown) are slightly weaker. The inter-annual variability of carbonate and lithogenic fluxes is the strongest factor in the inter-annual variability of the mass flux. For example, the maximum in mass flux of 1520 mg m^{-2} d^{-1} observed in December 2004 is to a large extent caused by a maximum in carbonate flux of 920 mg m^{-2} d^{-1}. On the other hand, the summer-autumn maximum in mass flux observed in 2005 is dominated the flux of lithogenic material of up to 240 mg m^{-2} d^{-1}.

Fluxes of alkenones and total isoprenoidal GDGTs (Figure 3c,e) also co-vary with mass flux and show a distinct seasonality with maxima during the “high flux periods” in the peak upwelling season and minima in the season of weaker upwelling. The GDGT flux is strongly correlated with mass flux (r^2=0.79), TOC flux (r^2=0.81) and opal flux (r^2=0.68) (Figure 4 e, f), while its correlation with carbonate flux is lower (r^2=0.52). In contrast, the correlations of alkenone flux with TOC flux (r^2=0.63) and mass flux (r^2=0.55; not shown) are less pronounced, as is its correlation with opal flux (r^2=0.6). The alkenone flux is only weakly correlated with carbonate flux (r^2=0.42; Figure 4d). Alkenone flux rates range between 0.8 and 38 mg m^{-2} d^{-1}. The GDGT flux is only given in arbitrary units due to the lack of an internal standard material at the time of analyses (see methods).

4.3 Seasonal variations of biomarker proxies in sinking particles

The four-year record of $U^{K'}_{37}$ is clearly seasonal with values ranging between 0.57 and 0.92 (±0.01), an amplitude of approximately 0.35 (Figure 3b). Maxima occur in autumn or winter (October to January), which is one to three months after SST (as determined by Advanced Very High Resolution Radiometer (AVHRR) at 20.45°N, 18.41°W) reaches maximum values (Figure 3a). Likewise, the minima in $U^{K'}_{37}$ are shifted by 1-3 months relative to the observed SST minima. The flux-weighted average $U^{K'}_{37}$ value over the investigated time period is 0.72 (Table 3).

The TEX_{86} record of the sinking particles collected in the sediment trap is presented in Figure 3d. A seasonal variability is clearly evident with values ranging between 0.55 and 0.67. Again, maxima and minima are delayed relative to the SST maxima and minima observed by satellite (Figure 3a), and the phase shift is even larger than the 1-3 months observed in the alkenone record. Notably, GDGT concentrations in particles sinking during the periods of low flux were often too low to permit determination of TEX_{86}. The flux weighted average TEX_{86} value (calculated only for the time period for which the GDGT flux was determined, namely CBeu-2 to CBeu-4 sample series) is 0.61, (Table 3). Branched GDGTs could not be detected in all samples. Where BIT index values could be calculated they are < 0.006 (not shown here).

4.4 Alkenone and GDGT composition of surface sediment

In the surface sediment (0-1 cm of multicore GeoB13612-3), a $U^{K'}_{37}$ value of 0.74 was measured. The surface sediment of GeoB13612-3 had a TEX_{86} value of 0.61 as reported previously (Basse *et al.*, 2014).

5. Discussion

5.1 Seasonality of lipid fluxes and estimated particle settling rates

All measured fluxes are seasonal in nature and reflect the productivity pattern at the Cape Blanc upwelling region (Figure 3). Highest total fluxes occur during or slightly after the season of strongest upwelling. In the summer/autumn (July to November) seasons of 2004 and 2006 all fluxes are low, whereas in 2003 and 2005, secondary flux maxima are observed between July and October. Winter 2004/2005 is characterized by an early high flux season during which the highest total fluxes of the entire study period are observed. Alkenone and GDGT fluxes are correlated with mass flux. This correlation, however, does not unambiguously prove that production of these lipids has the same

seasonal variability as mass flux resulting from total primary productivity. Rather, fluxes of lipids could be strongly controlled by how and into what type of sinking particles the respective lipids are incorporated (cf. Rosell-Melé and Prahl, 2013; Wuchter *et al.*, 2006), i.e. the fluxes of alkenones and GDGTs are high at the peak in mass flux because this acts as an important mechanisms for transporting these lipids to the seafloor and not because their concentration in SPM are highest at that time.

In general, the seasonal variations in $U^{K'}_{37}$ and TEX_{86} resemble the seasonal changes in SST. However, the maxima and minima of the respective index values are delayed with respect to those of satellite SST (Figure 3). This is a well-known phenomenon and has been observed in many sediment trap studies for $U^{K'}_{37}$ (e.g., Müller and Fischer, 2003) as well as for TEX_{86} (Wuchter *et al.*, 2006), where it has been explained as being due to slow sinking of particles through the water column. Consequently, the delays have been used to estimate sinking velocities of particles containing the respective lipids. For this purpose, the mooring depth of the trap is divided by the time lag between maximum (minimum) temperatures of satellite measurements and the consecutive collection period of the sediment trap in which the highest (lowest) $U^{K'}_{37}$ or TEX_{86} values are recorded (cf. Fischer and Karakas, 2009). It has to be noted, though, that by using this approach, the time required for lipids to be incorporated into sinking particles prior to being exported will not be considered separately (see also discussion below). The time period used to calculate sinking velocities thus includes the time before the formation of a sinking particle as well as the actual sinking process. At our trap site, we thus determine sinking rates for alkenone-containing particles of 17-59 m d^{-1} for the summer and from 14-30 m d^{-1} for the cold upwelling season. It has to be noted that sinking rates for the cold upwelling season are rather difficult to determine and thus need to be regarded less reliable, as the minima in the $U^{K'}_{37}$ (and TEX_{86}) record are not well pronounced due to low lipid concentrations in the respective samples that did not always allow the determination of an index value. This implies that alkenone (and GDGT) production during peak upwelling is reduced, or export of the respective lipids is less efficient due to a lower total flux.

The sinking rates we determined for alkenones are considerably lower than rates reported for a nearby location in the mesotrophic filamentous region off Cape Blanc, where Müller and Fischer (2001) reported sinking rates of 80 and 280 m d^{-1} for the low and high particle flux periods, respectively. For the same site, Fischer and Karakaş

(2009) reported sinking rates of 95-130 m d^{-1} determined from mass flux patterns. Lower values were observed during a diatom-rich winter-spring bloom, while the higher values were determined for particles dominated by coccolithophorids sinking during summer. This is in agreement with experimental data suggesting that particles containing coccolithophorids sink faster than particles containing diatoms (Iversen *et al.*, 2010). Higher relative abundances of diatoms in sinking particles containing both coccolithophorid and diatom detritus at our eutrophic study site might thus account for the lower rates observed here than published rates for the mesotrophic location.

When assuming predominant export of GDGTs from near-surface waters, sinking rates (including time of formation of a sinking particle) determined for GDGT containing particles are substantially lower than for alkenones and vary between 9-17 m d^{-1}, suggesting that these lipids are transported in the water column via other particle types than the alkenones. Together with the strong correlation of GDGT fluxes with opal and mass fluxes (Figure 4), this suggests that export of these lipids is generally tied to diatom-dominated fluxes. A similar observation was made in the North Pacific, where the authors noted good correlations of GDGT fluxes with those of TOC, opal and lithogenic particles and hypothesized that GDGTs sank with the main components of organic material (Yamamoto *et al.*, 2012).

It is known that sinking rates of particles increase with increasing depth (Berelson, 2001; Fischer and Karakas, 2009), and sinking rates calculated in the manner described above are average values for the entire water column interval between the depth of production (surface) and the mooring depth of the sediment trap. A plausible scenario explaining this observation is that the average time a particle remains in suspension until it is incorporated in sinking particles (i.e., faecal pellets or marine snow aggregates of sufficient density) differs between water depths, and likely also between particle types. The time differences between observed SST maxima and minima and index maxima and minima are therefore probably more accurately described as delays in export.

For GDGT containing particles, the time period between formation and export may be up to 4 months, if high sinking rates are assumed for particles sinking below the zone of aggregation. It is conceivable that the average time period passing before the GDGTs produced in near-surface waters become incorporated into sinking particles depends also on the total flux in the region. In upwelling regions with pronounced seasonal flux peaks like our study region, GDGTs in the surface waters might be effectively scavenged

and "rained out" during those seasonal peaks, whereas in more oligotrophic regions lacking sufficient ballasting material, the average residence time of GDGTs in surface waters might be longer. The observed seasonality in GDGT fluxes alone therefore does not provide evidence for or against a distinct cycle in seasonal abundance of Thaumarchaeota.

5.2 Comparison of reconstructed and satellite SST

5.2.1 Alkenone thermometry

$U^{K'}_{37}$-based SST reconstructions from the sinking particles collected in the sediment trap show a pronounced seasonality (Figure 3b). Reconstructed temperatures using the calibration for SPM from surface waters (Eq. 2) published by Conte et al. (2006) are in excellent agreement with observed SST (Figure 5a) with respect to the seasonal amplitude, and $U^{K'}_{37}$ values of our SPM samples lie within the scatter of SPM values used for determining the calibration, suggesting that the SPM calibration yields realistic surface temperature estimates in our study region (Figure 2a). This is remarkable because data from upwelling sites in the NE Atlantic have been excluded from the calibration data set because they were regarded anomalous (Conte *et al.*, 2006). If the core-top calibration (Eq.3) from the same publication is used, $U^{K'}_{37}$-derived SST minima are up to 3.9°C colder than satellite data (Figure 5b), while maxima correspond rather well with observations. This discrepancy between the calibrations for SPM and for core-top sediments is well known and has been ascribed to a combination of seasonal production of alkenones and differential degradation of the two alkenones used in the index during sinking or at the sediment surface (Conte *et al.*, 2006 and references therein). Our observation suggests that the initial $U^{K'}_{37}$ signatures of particles formed in surface waters at our study site remains intact during sinking, at least down to approximately 1300m, where our sediment trap was moored. Any modification by degradation of the two alkenones $C_{37:3}$ and $C_{37:2}$ at differential rates must thus occur either during further sinking through the deeper water column (below 1300 m) or at the water-sediment interface and in the surface sediment. The latter is regarded to be the more likely scenario, as particle sinking rates in the deeper parts of the water column are much faster than near the surface (e.g., Fischer and Karakas, 2009) and degradation of organic matter is strongly reduced (Iversen and Ploug, 2013). Selective degradation of the tri-unsaturated relative to the di-unsaturated alkenones has been suggested as the

498 cause for diagenetic increases of the $U_{37}^{K'}$ signal occurring upon prolonged exposure to
499 oxygen rich bottom waters , (Gong and Hollander, 1999; Hoefs *et al.*, 1998). The
500 alkenones will be exposed to oxygen for a much longer time in the sediment than during
501 transport in the water column, therefore alteration of the $U_{37}^{K'}$ in the sediment is more
502 likely, in agreement with our findings.
503 The $U_{37}^{K'}$ index in the underlying surface sediment is 0.74, which is slightly higher
504 than the flux-weighted average value for the trap samples of 0.72 (Table 3). This would
505 be expected if sinking particles retain a surface water signal, while sediments that
506 integrate over several millennia contain alkenones at relative abundance influenced by
507 differential degradation. While the difference of 0.02 units between the two values is
508 close to the analytical uncertainty, the expected $U_{37}^{K'}$ values using the SPM and surface
509 sediment calibrations for an annual mean SST of 21.2°C would be 0.72 and 0.75,
510 respectively in remarkable agreement with our observations. Moreover, a slight bias
511 towards the colder high productivity season in our study area would be expected in the
512 $U_{37}^{K'}$ value of the surface sediment, which is in agreement with the observed value of
513 0.74, slightly lower than the expected $U_{37}^{K'}$ value for an annual mean SST of 21.2°C. No
514 bias towards the colder upwelling season is observed in the flux weighted average value
515 of the sinking particles collected in the trap. This might either suggest that the slightly
516 cooler surface sediment signal is due to uncertainty of the method, or a better
517 preservation of alkenones exported to the sediment during high flux periods than those
518 reaching the sea floor under low flux conditions.
519
520 *5.2.2 TEX_{86} thermometry*
521 TEX_{86} values of the SPM collected during our study display a temperature
522 relationship with *in situ* water temperature that is in moderate agreement with the
523 empirical relationship observed for SPM <100 m (Eq. 8; Figure 2b) (Schouten *et al.*,
524 2013b), but TEX_{86} values tend to be lower than predicted from the regression. Our
525 surface water SPM samples were collected at SSTs ranging between 18.3 and 23.3°C
526 (Table 2). This is within the temperature range for which the use of the logarithmic
527 temperature calibration (Eq. 6) is recommended (Kim *et al.*, 2010). The good agreement
528 of our data with the data by Kim *et al.* (2010) suggests that this calibration can be
529 applied with confidence in this study area (Figure 2d).

When applying the calibration Schouten et al. (2013b) proposed for TEX_{86} of SPM from <100 m (Eq. 8) to the data obtained from the sediment trap samples, the TEX_{86}-temperatures range between 16.7 and 21.6 °C (Figure 5c). These estimates are much lower than observed SST at the trap site. TEX_{86}-temperatures estimated seasonal amplitudes of ~4 °C (compared to ~7 °C in the observed SST), and maxima (minima) that are roughly 4.5 °C (1.5°C) colder than the maxima and minima in the observed SST. An underestimation of SST could be expected, as the surface water SPM collected in our study region cluster below the calibration line (Figure 2b). Lower than expected TEX_{86}-temperatures have often be attributed to export of GDGTs from deeper and cooler waters than the surface (cf. Kim *et al.*, 2012). However, TEX_{86}-values of SPM collected in 2009, 2010, 2011 and 2012 throughout the water column at our trap station using in-situ pumps showed a distinct maximum below the chlorophyll maximum and above 1000 m, coincident with an intermediate nepheloid layer and a minimum in oxygen concentration (Basse *et al.*, 2014). Export from deeper waters can therefore not explain the observed mismatch between the temperature reconstructions based on the SPM calibration from Schouten et al. (2013b) and the observed SST. The reported SPM calibration is therefore probably not suitable for the sinking particles collected at the study site off Cape Blanc.

When calculating TEX_{86}- temperatures from our data from the sinking particles using the core-top calibration (Eq. 6, Kim *et al.*, 2010), the reconstructed temperatures display a reduced seasonal amplitude (~4°C) compared with the satellite based SST (seasonal amplitude of ~7°C) (Figure 5d). Reconstructed maxima of ~26°C are slightly higher but well within calibration error of ±2.5°C (Kim *et al.*, 2010) of the observed maxima of up to 25.3°C. The reconstructed temperature minima of 21.4-22.1°C, however, are higher than observed minima which reach 18.5°C. Thus, TEX_{86}- temperature estimates of sinking particles, its flux-weighted mean, and of surface sediments (23.9°C for sediment and flux-weighted mean) are high compared with measured SST values (annual mean of 21.2°C).

The use of a different temperature calibration has been proposed to account for warmer than expected TEX_{86}- temperatures reconstructed from sediments. Kim *et al.* (2012) studied a sediment core recovered from 2500 m water depth at a site off Mauritania approximately 65 km from our trap site. When using the logarithmic calibration (Eq. 6) of Kim *et al.* (2010), TEX_{86}- temperatures were higher than $U^{K'}_{37}$-

temperatures for the same core. In order to reconcile this, the authors suggested that TEX_{86} corresponded to depth-integrated annual temperatures from 0 to 200 m water depth rather than to annual mean SST. As seasonally resolved mean temperatures of the upper 200 m water depth at the trap site are not available for the time of sample collection with the sediment trap, we cannot test this relationship for our samples. However, when converting the flux-weighted mean TEX_{86} of 0.61 to temperature using the 0-200m calibration (Eq.7) proposed by Kim *et al.* (2012), the resulting temperature estimate is ca. 19 °C. This is similar to the World Ocean Atlas annual mean value for 0-200 m of approximately 18.5°C (Locarnini *et al.*, 2010).

Alternatively, a mismatch between TEX_{86}-temperatures and observed SST could be related to lateral advection. If lateral advection occurred, the likely source area of particles transported to the study site located within the filamentous cold water tongue would be the near-shore areas with highest productivity. These areas are characterized by lower SST, thus, a "cold" rather than the observed "warm bias" would be expected. Moreover, alkenones would be affected by the same lateral advection process, likely even more strongly as they are inferred to be more susceptible than isoprenoidal GDGTs to long-range transport in oxygen-replete water masses (Mollenhauer *et al.*, 2008). Yet, as discussed above the $U^{K'}_{37}$ record reflects local SST rather well. We therefore infer that lateral advection does not play an important role in our study area.

A warm bias in the reconstructed temperature could be related to increased abundance of Thaumarchaeota during the summer warm season. Those samples of sinking particles collected in low flux periods, which contained sufficient GDGTs for a TEX_{86} measurement, yielded low values, translating to the TEX_{86}-temperature minima. The sinking particles collected during the peak flux periods corresponding to times of highest primary production due to upwelling, however, tend to have higher TEX_{86} values. The TEX_{86} results from our SPM samples and these flux data taken together are consistent with a scenario where GDGT producers are most abundant in the warm, non-upwelling season of the year. However, they cannot be exported during this time period due to a lack of aggregate formation or zooplankton grazing. Higher particle abundances following phytoplankton blooms during the upwelling season would then lead to a more effective scavenging of GDGTs from the surface waters during the high flux season, resulting in a delayed export. The TEX_{86} signal carried by these particles would still be dominated by material produced during the warm season, as higher abundances of Thaumarchaeota during the non-upwelling phase would effectively override a signal

produced during upwelling, when Thaumarchaeota are not competitive and therefore less abundant. Contrasting seasonality of phytoplankton and Thaumarchaeota has previously been observed elsewhere (e.g ., Herfort *et al.*, 2006). A better correspondence between TEX_{86}- temperature estimates and summer temperature has been suggested for the Mediterranean (Castañeda *et al.*, 2010), in agreement with our observations.

The scenario of delayed export of GDGTs suggests that sinking particles should contain a TEX_{86} value that integrates over a certain time period. This is in agreement with observations made in other studies on sinking particles collected by sediment traps, where in particular in deeper traps, TEX_{86} corresponds to an annually averaged SST (Fallet *et al.*, 2011; Wuchter *et al.*, 2006; Yamamoto *et al.*, 2012). It also suggests that the process of GDGT scavenging by aggregates or packaging into faecal pellets takes sufficiently long to result in sinking particles carrying integrated TEX_{86} signals, which results in an attenuation of seasonal cycles.

As introduced above, TEX_{86}-values of SPM collected throughout the water column at our trap station showed a distinct maximum below the chlorophyll maximum and above 1000 m, coincident with an intermediate nepheloid layer and reduced oxygen concentrations (Basse *et al.*, 2014). This maximum in TEX_{86} was hypothesized to be attributable to production of GDGTs by a metabolically and, perhaps, also genetically distinct planktonic archaeal community thriving in these depths. Interestingly, the concentration-weighted mean value of SPM-TEX_{86} from the entire water column at our trap site was 0.61 (Basse *et al.*, 2014), which again is identical to both the flux-weighted average TEX_{86} from the sediment trap and the surface sediment value from underlying site GeoB13612-3. Export of GDGTs produced by a community thriving in low-oxygen waters between 200 and 1000 m, carrying a "warm" TEX_{86} signal and contributing to total vertical GDGT flux is thus a plausible alternative scenario at our sediment trap location. As similar deep-water maxima have so far been reported from sites with oxygen minima in corresponding water depths (Schouten *et al.*, 2012; Xie *et al.*, 2014), it is possible that such a warm bias could only be expected in regions where oxygen-deficient deep waters are present. Nearby locations without oxygen minima might not be affected.

Finally, the fact that identical TEX_{86} values of 0.61 were determined as flux-weighted mean of the sinking particles as well as for the underlying surface sediments suggests that, unlike the $U^{K'}_{37}$ index, TEX_{86} does not undergo significant alteration during

sinking and early diagenesis in surface sediments. Previous studies have not found a significant bias of TEX_{86} due to early diagenetic alteration either (Huguet *et al.*, 2006a; Kim *et al.*, 2009; Schouten *et al.*, 2004; Yamamoto *et al.*, 2012).

6. Conclusions

The four-year record of particle and lipid fluxes and of the $U^{K'}_{37}$ and TEX_{86} indices in the eutrophic filamentous zone off Cape Blanc indicates that alkenone and GDGT production and export vary seasonally. Export of lipids is delayed relative to the time of production, and the delay is longer for GDGTs than for alkenones. This translates into slower average sinking rates (0-1300 m) for particles containing GDGTs (9-17 m d^{-1}) than for alkenones (14-59 m d^{-1}). The latter is slower than published values for a nearby mesotrophic site, suggesting that differing particle composition with more diatom rich aggregates at the higher productivity site determines the sinking rates. GDGTs are likely exported predominantly within opal-rich aggregates.

SST reconstructions based on alkenones are in excellent agreement with satellite data, and the entire seasonal amplitude of temperature variations at the sea surface is well recorded. In contrast, GDGT based temperature reconstructions using the logarithmic TEX_{86} calibration yields temperature maxima similar to observed maxima, but a reduced seasonal amplitude. This observation is in agreement with predominant Thaumarchaeotal production during the warm season and near the sea surface, or with contributions from subsurface communities with a GDGT distribution resulting in a high TEX_{86} signal.

The data discussed in this publication are archived in the data center "Pangaea" (doi:10.1594/PANGAEA.835471; www.Pangaea.de).

Acknowledgements

We thank the captains, crews and chief scientists of R/V Meteor cruises 58/2 and 65/2, R/V Poseidon cruises 310 and 344, and R/V Merian cruises 04b and 11-2. Marco Klann, Hella Buschoff and Ralph Kreutz are thanked for laboratory assistance. The research leading to these results has received funding from the Deutsche Forschungsgemeinschaft via MARUM, the Helmholtz-Association through a Young Investigators Group grant to GM, and the European Research Council under the European Union's Seventh Framework Programme (FP7/2007-2013) / ERC grant

664 agreement n° [226600] to JSSD. We thank three anonymous reviewers, whose
665 constructive comments helped improve the manuscript.

666

667 **References**

668 Basse, A., Zhu, C., Versteegh, G.J.M., Fischer, G., Hinrichs, K.-U., Mollenhauer, G., 2014.
669 Distribution of intact and core tetraether lipids in water column profiles of
670 suspended particulate matter off Cape Blanc, NW Africa. Organic Geochemistry 72
671 (0), 1-13.
672 Behrenfeld, M.J., Falkowski, P.G., 1997. Photosynthetic rates derived from satellite-based
673 chlorophyll concentration. Limnology and Oceanography 42 (1), 1-20.
674 Berelson, W.M., 2001. Particle settling rates increase with depth in the ocean. Deep Sea
675 Research Part II: Topical Studies in Oceanography 49, 237-251.
676 Bickert, T., Braun, S., Fricke, S., Hermann, B., Just, J., Keil, H., Klann, M., Krastel, S.,
677 Kurschat, S., Mai, A., Meyer, I., Meyer, M., Mollenhauer, G., Nowald, N., Ruhland, G.,
678 Schilling, S., Schwab, A., Schwenk, T., Stuut, J.-B., Vega, D., 2011. Pre-site survey for
679 an IODP cruise; Neogene Paleoclimate and sediment transport at the continental
680 margin of NW Africa - Cruise No. MSM11/2 - March 14 - April 09, 2009 - Dakar
681 (Senegal) - Las Palmas (Canary Islands, Spain). Maria S. Merian-Berichte. DFG
682 Senatskommission for Ozeanographie, p. 53.
683 Brassell, S.C., Eglinton, G., Marlowe, I.T., Pflaumann, U., Sarnthein, M., 1986. Molecular
684 stratigraphy: a new tool for climatic assessment. Nature 320, 129-133.
685 Brochier-Armanet, C., Boussau, B., Gribaldo, S., Forterre, P., 2008. Mesophilic
686 crenarchaeota: proposal for a third archaeal phylum, the Thaumarchaeota. Nat Rev
687 Micro 6 (3), 245-252.
688 Carr, M.-E., Friedrichs, M.A.M., Schmeltz, M., Noguchi Aita, M., Antoine, D., Arrigo, K.R.,
689 Asanuma, I., Aumont, O., Barber, R., Behrenfeld, M., Bidigare, R., Buitenhuis, E.T.,
690 Campbell, J., Ciotti, A., Dierssen, H., Dowell, M., Dunne, J., Esaias, W., Gentili, B.,
691 Gregg, W., Groom, S., Hoepffner, N., Ishizaka, J., Kameda, T., Le Quéré, C., Lohrenz, S.,
692 Marra, J., Mélin, F., Moore, K., Morel, A., Reddy, T.E., Ryan, J., Scardi, M., Smyth, T.,
693 Turpie, K., Tilstone, G., Waters, K., Yamanaka, Y., 2006. A comparison of global
694 estimates of marine primary production from ocean color. Deep Sea Research Part
695 II: Topical Studies in Oceanography 53 (5,Äì7), 741-770.
696 Castañeda, I.S., Schefuß, E., Pätzold, J., Sinninghe Damsté, J.S., Weldeab, S., Schouten, S.,
697 2010. Millennial-scale sea surface temperature changes in the eastern
698 Mediterranean (Nile River Delta region) over the last 27,000 years.
699 Paleoceanography 25 (1), PA1208.
700 Chen, W., Mohtadi, M., Schefuß, E., Mollenhauer, G., 2014. Organic-geochemical proxies
701 of sea surface temperature in surface sediments of the tropical eastern Indian
702 Ocean. Deep Sea Research Part I: Oceanographic Research Papers 88 (0), 17-29.
703 Conte, M., Sicre, M.A., Rühlemann, C., Weber, J.C., Schulte, S., Schulz-Bull, D.E., Blanz, T.,
704 2006. Global temperature calibration of the alkenone unsaturation index ($U^{K'}_{37}$) in
705 surface waters and comparison with surface sediments. Geochemistry, Geophysics,
706 Geosystems, G3 7 (2), doi:10.1029/2005GC001054.
707 Etourneau, J., Collins, L.G., Willmott, V., Kim, J.H., Barbara, L., Leventer, A., Schouten, S.,
708 Sinninghe Damsté, J.S., Bianchini, A., Klein, V., Crosta, X., Massé, G., 2013. Holocene
709 climate variations in the western Antarctic Peninsula: evidence for sea ice extent
710 predominantly controlled by changes in insolation and ENSO variability. Clim. Past
711 9 (4), 1431-1446.

712 Fallet, U., Ullgren, J.E., Castañeda, I.S., van Aken, H.M., Schouten, S., Ridderinkhof, H.,
713 Brummer, G.-J.A., 2011. Contrasting variability in foraminiferal and organic
714 paleotemperature proxies in sedimenting particles of the Mozambique Channel
715 (SW Indian Ocean). Geochimica et Cosmochimica Acta 75 (20), 5834-5848.
716 Fischer, G. and cruise participants 2011. Report and preliminary results of RV Poseidon
717 cruise 396, Las Palmas - Las Palmas, 24.2.-8.3.2010. Berichte Fachbereich
718 Geowissenschaften 277, 22.
719 Fischer, G., Karakas, G., 2009. Sinking rates and ballast composition of particles in the
720 Atlantic Ocean: implications for the organic carbon fluxes to the deep ocean.
721 Biogeoscienes 6, 85-702.
722 Fischer, G., Wefer, G., 1991. Sampling, preparation and analysis of marine particulate
723 matter. Marine particles: Analysis and Characterization. AGU, Washington, DC, pp.
724 391-397.
725 Fréon, P., Arístegui, J., Bertrand, A., Crawford, R.J.M., Field, J.C., Gibbons, M.J., Tam, J.,
726 Hutchings, L., Masski, H., Mullon, C., Ramdani, M., Seret, B., Simier, M., 2009.
727 Functional group biodiversity in Eastern Boundary Upwelling Ecosystems
728 questions the wasp-waist trophic structure. Progress in Oceanography 83 (1-4),
729 97-106.
730 Gong, C., Hollander, D., 1999. Evidence for differential degradation of alkenones under
731 contrasting bottom water oxygen conditions: Implication for paleotemperature
732 reconstruction. Geochimica et Cosmochimica Acta 63 (3/4), 405-411.
733 Grice, K., Klein Breteler, W.C.M., Schouten, S., Grossi, V., de Leeuw, J.W., Damsté, J.S.S.,
734 1998. Effects of zooplankton herbivory on biomarker proxy records.
735 Paleoceanography 13 (6), 686-693.
736 Herfort, L., Schouten, S., Boon, J.P., Sinninghe Damsté, J.S., 2006. Application of the TEX_{86}
737 temperature proxy to the southern North Sea. Organic Geochemistry 37 (12), 1715.
738 Hoefs, M.J.L., Versteegh, G.J.M., Rijpstra, W.I.C., de Leeuw, J.W., Sinninghe Damsté, J.S.,
739 1998. Postdepositional oxic degradation of alkenones: Implications for the
740 measurement of palaeo sea surface temperatures. Paleoceanography 13 (1), 42-49.
741 Hopmans, E.C., Schouten, S., Pancost, R.D., van der Meer, M.T.J., Sinninghe Damsté, J.S.,
742 2000. Analysis of intact tetraether lipids in archaeal cell material and sediments by
743 high performance liquid chromatography/atmospheric pressure chemical
744 ionization mass spectrometry. Rapid Communications in Mass Spectrometry 14,
745 585-589.
746 Hopmans, E.C., Weijers, J.W.H., Schefuß, E., Herfort, L., Sinninghe Damsté, J.S., Schouten,
747 S., 2004. A novel proxy for terrestrial organic matter in sediments based on
748 branched and isoprenoid tetraether lipids. Earth and Planetary Science Letters 224,
749 107-116.
750 Huguet, C., Cartes, J.E., Sinninghe Damsté, J.S., Schouten, S., 2006a. Marine
751 creanarchaeotal membrane lipids in decapods: Implications for the TEX_{86}
752 paleothermometer. Geochemistry, Geophysics, Geosystems, G3 7 (11), Q11010.
753 Huguet, C., Kim, J.-H., Sinninghe Damsté, J.S., Schouten, S., 2006b. Reconstruction of sea
754 surface temperature variations in the Arabian Sea over the last 23 kyr using
755 organic proxies (TEX_{86} and $U^{K'}_{37}$). Paleoceanography 21, PA3003.
756 Huguet, C., Schimmelmann, A., Thunell, R., Lourens, L.J., Sinninghe Damsté, J.S., Schouten,
757 S., 2007. A study of the TEX_{86} paleothermometer in the water column and
758 sediments of Santa Barbara Basin, California. Paleoceanography 22, PA3203.
759 Iversen, M.H., Nowald, N., Ploug, H., Jackson, G.A., Fischer, G., 2010. High resolution
760 profiles of vertical particulate organic matter export off Cape Blanc, Mauritania:

761 Degradation processes and ballasting effects. Deep Sea Research Part I:
762 Oceanographic Research Papers 57 (6), 771-784.
763 Iversen, M.H., Ploug, H., 2010. Ballast minerals and the sinking carbon flux in the ocean:
764 carbon-specific respiration rates and sinking velocity of marine snow aggregates.
765 Biogeosciences 7, 2613-2624.
766 Iversen, M.H., Ploug, H., 2013. Temperature effects on carbon-specific respiration rate
767 and sinking velocity of diatom aggregates - potential implications for deep ocean
768 export processes. Biogeosciences 10 (6), 4073-4085.
769 Karner, M.B., DeLong, E.F., Karl, D.M., 2001. Archaeal dominance in the mesopelagic zone
770 of the Pacific Ocean. Nature 409, 507-510.
771 Kienast, M., Kienast, S.S., Calvert, S.E., Eglinton, T.I., Mollenhauer, G., François, R., Mix, A.,
772 2006. Eastern Pacific cooling and Atlantic overturning circulation during the last
773 deglaciation. Nature 443, 846-849.
774 Kim, J.-H., Huguet, C., Zonneveld, K.A.F., Versteegh, G.J.M., Roeder, W., Sinninghe Damsté,
775 J.S., Schouten, S., 2009. An experimental field study to test the stability of lipids
776 used for the TEX_{86} and $U^{K'}_{37}$palaeothermometers. Geochimica et Cosmochimica
777 Acta 73 (10), 2888-2898.
778 Kim, J.-H., Romero, O.E., Lohmann, G., Donner, B., Laepple, T., Haam, E., S., S.D.J., 2012.
779 Pronounced subsurface cooling of North Atlantic waters off Northwest Africa
780 during Dansgaard-Oeschger interstadials. Earth and Planetary Science Letters 339-
781 340 (0), 95-102.
782 Kim, J.-H., van der Meer, J., Schouten, S., Helmke, P., Willmott, V., Sangiorgi, F., Koç, N.,
783 Hopmans, E.C., Damsté, J.S.S., 2010. New indices and calibrations derived from the
784 distribution of crenarchaeal isoprenoid tetraether lipids: Implications for past sea
785 surface temperature reconstructions. Geochimica et Cosmochimica Acta 74 (16),
786 4639-4654.
787 Lamy, F., Kaiser, J., Ninnemann, U., Hebbeln, D., Arz, H.W., Stoner, J.S., 2004. Antarctic
788 timing of surface water change off Chile and Patagonian Ice Sheet response.
789 Science 304, 1959-1962.
790 Lathuilière, C., Echevin, V., Lévy, M., 2008. Seasonal and intraseasonal surface
791 chlorophyll-a variability along the northwest African coast. Journal of Geophysical
792 Research: Oceans 113 (C5), C05007.
793 Lee, K.E., Kim, J.-H., Wilke, I., Helmke, P., Schouten, S., 2008. A study of the alkneone,
794 TEX_{86}, and planktonic foraminifera in the Bengulea Upwelling System: Implications
795 for past sea surface temperature estimates. Geochemistry, Geophysics, Geosystems,
796 G3 9 (10), Q10019.
797 Leider, A., Hinrichs, K.-U., Mollenhauer, G., Versteegh, G.J.M., 2010. Core-top calibration
798 of the lipid-based and TEX_{86} temperature proxies on the southern Italian shelf (SW
799 Adriatic Sea, Gulf of Taranto). Earth and Planetary Science Letters 300 (1-2), 112-
800 124.
801 Locarnini, R.A., Mishonov, A.V., Antonov, J.I., Boyer, T.P., Garcia, H.E., Baranova, O.K.,
802 Zweng, M.M., Johnson, D.R., 2010. World ocean Atlas 2009, Volume 1: Temperature.
803 In: Levitus, S. (Ed.), NOAA Atlas NESDIS 68. U.S. Government Printing Office,
804 Washington, D.C., p. 184.
805 Lopes dos Santos, R.A., Prange, M., Castañeda, I.S., Schefuß, E., Mulitza, S., Schulz, M.,
806 Niedermeyer, E.M., Sinninghe Damsté, J.S., Schouten, S., 2010. Glacial-interglacial
807 variability in Atlantic meridional overturning circulation and thermocline
808 adjustments in the tropical North Atlantic. Earth and Planetary Science Letters 300
809 (3-4), 407-414.

Lopes dos Santos, R.A., Spooner, M.I., Barrows, T.T., De Deckker, P., Sinninghe Damsté, J.S., Schouten, S., 2013. Comparison of organic ($U^{K'}_{37}$, $TEXH_{86}$, LDI) and faunal proxies (foraminiferal assemblages) for reconstruction of late Quaternary sea surface temperature variability from offshore southeastern Australia. Paleoceanography 28 (3), 377-387.

Martínez-Garcia, A., Rosell-Melé, A., Geibert, W., Gersonde, R., Masqué, P., Gaspari, V., Barbante, C., 2009. Links between iron supply, marine productivity, sea surface temperature, and CO_2 over the last 1.1 Ma. Paleoceanography 24 (1), PA1207.

McClymont, E.L., Ganeshram, R.S., Pichevin, L.E., Talbot, H.M., van Dongen, B.E., Thunell, R.C., Haywood, A.M., Singarayer, J.S., Valdes, P.J., 2012. Sea-surface temperature records of Termination 1 in the Gulf of California: Challenges for seasonal and interannual analogues of tropical Pacific climate change. Paleoceanography 27 (2), PA2202.

Meunier, T., Barton, E.D., Barreiro, B., Torres, R., 2012. Upwelling filaments off Cap Blanc: Interaction of the NW African upwelling current and the Cape Verde frontal zone eddy field? Journal of Geophysical Research: Oceans 117 (C8), C08031.

Mittelstaedt, E., 1991. The ocean boundary along the northwest African coast: Circulation and oceanographic properties at the sea surface. Progress in Oceanography 26 (4), 307-355.

Mollenhauer, G., Eglinton, T.I., Hopmans, E.C., Sinninghe Damsté, J.S., 2008. A radiocarbon-based assessment of the preservation characteristics of crenarchaeol and alkenones from continental margin sediments. Organic Geochemistry 39 (8), 1039-1045.

Müller, P.J., Fischer, G., 2001. A 4-year sediment trap record of alkenones from the filamentous upwelling region off Cape Blanc, NW Africa and a comparison with distributions in underlying sediments. Deep Sea Research Part I: Oceanographic Research Papers 48 (8), 1877.

Müller, P.J., Fischer, G., 2003. C_{37}-Alkenones as paleotemperature tool: Fundamentals based on sediment traps and surface sediments form the South Atlantic Ocean. In: Wefer, G., Mulitza, S., Rathmeyer, V. (Eds.), The South Atlantic in the Late Quaternary: Reconstruction of Material Budgets and Current Systems. Springer, Berlin, pp. 167-193.

Müller, P.J., Kirst, G., Ruhland, G., von Storch, I., Rosell-Melé, A., 1998. Calibration of the alkenone paleotemperature index $U^{K'}_{37}$ based on core tops from the eastern South Atlantic and the global ocean. Geochimica et Cosmochimica Acta 62 (10), 1757-1772.

Müller, P.J., Schneider, R., 1993. An automated leaching method for the determination of opal in sediments and particulate matter. Deep Sea Research Part I: Oceanographic Research Papers 40 (3), 425-444.

Pradhan, Y., Lavender, S.J., Hardman-Mountford, N.J., Aiken, J., 2006. Seasonal and inter-annual variability of chlorophyll-a concentration in the Mauritanian upwelling: Observation of an anomalous event during 1998-1999. Deep Sea Research Part II: Topical Studies in Oceanography 53 (14,Äì16), 1548-1559.

Prahl, F.G., Wakeham, S.G., 1987. Calibration of unsaturation patterns in long-chain ketone compositons for palaeotemperature assessment. Nature 330, 367-369.

Rommerskirchen, F., Condon, T., Mollenhauer, G., Dupont, L., Schefuß, E., 2011. Miocene to Pliocene development of surface and subsurface temperatures in the Benguela Current system. Paleoceanography 26 (3), PA3216.

Rosell-Melé, A., Prahl, F.G., 2013. Seasonality of temperature estimates as inferred from sediment trap data. Quaternary Science Reviews 72 (0), 128-136.

Rühlemann, C., Mulitza, S., Müller, P.J., Wefer, G., 1999. Warming of the tropical Atlantic Ocean and slowdown of thermohaline circulation during the last deglacialtion. Nature 402, 511-514.
Schneider, B., Leduc, G., Park, W., 2010. Disentangling seasonal signals in Holocene climate trends by satellite-model-proxy integration. Paleoceanography 25 (4), PA4217.
Schouten, S., Forster, A., Panoto, F.E., Sinninghe Damsté, J.S., 2007. Towards calibration of the TEX_{86} palaeothermometer for tropical sea surface temperatures in ancient greenhouse worlds. Organic Geochemistry 38 (9), 1537.
Schouten, S., Hopmans, E.C., Rosell-Melé, A., Pearson, A., Adam, P., Bauersachs, T., Bard, E., Bernasconi, S.M., Bianchi, T.S., Brocks, J.J., Carlson, L.T., Castañeda, I.S., Derenne, S., Selver, A.D., Dutta, K., Eglinton, T., Fosse, C., Galy, V., Grice, K., Hinrichs, K.-U., Huang, Y., Huguet, A., Huguet, C., Hurley, S., Ingalls, A., Jia, G., Keely, B., Knappy, C., Kondo, M., Krishnan, S., Lincoln, S., Lipp, J., Mangelsdorf, K., Martínez-García, A., Ménot, G., Mets, A., Mollenhauer, G., Ohkouchi, N., Ossebaar, J., Pagani, M., Pancost, R.D., Pearson, E.J., Peterse, F., Reichart, G.-J., Schaeffer, P., Schmitt, G., Schwark, L., Shah, S.R., Smith, R.W., Smittenberg, R.H., Summons, R.E., Takano, Y., Talbot, H.M., Taylor, K.W.R., Tarozo, R., Uchida, M., van Dongen, B.E., Van Mooy, B.A.S., Wang, J., Warren, C., Weijers, J.W.H., Werne, J.P., Woltering, M., Xie, S., Yamamoto, M., Yang, H., Zhang, C.L., Zhang, Y., Zhao, M., Damsté, J.S.S., 2013a. An interlaboratory study of TEX_{86} and BIT analysis of sediments, extracts, and standard mixtures. Geochemistry, Geophysics, Geosystems 14 (12), 5263-5285.
Schouten, S., Hopmans, E.C., Schefuß, E., Sinninghe Damsté, J.S., 2002. Distributional variations in marine crenarchaeotal membrane lipids: a new tool for reconstructing ancient sea water temperatures? Earth and Planetary Science Letters 204, 265-274.
Schouten, S., Hopmans, E.C., Sinninghe Damsté, J.S., 2004. The effect of maturity and depositional redox conditions on archaeal tetraether lipid palaeothermometry. Organic Geochemistry 35 (5), 567-571.
Schouten, S., Hopmans, E.C., Sinninghe Damsté, J.S., 2013b. The organic geochemistry of glycerol dialkyl glycerol tetraether lipids: A review. Organic Geochemistry 54 (0), 19-61.
Schouten, S., Pitcher, A., Hopmans, E.C., Villanueva, L., van Bleijswijk, J., Sinninghe Damsté, J.S., 2012. Intact polar and core glycerol dibiphytanyl glycerol tetraether lipids in the Arabian Sea oxygen minimum zone: I. Selective preservation and degradation in the water column and its consequences for the TEX_{86}. Geochimica et Cosmochimica Acta (0).
Shevenell, A.E., Ingalls, A.E., Domack, E.W., Kelly, C., 2011. Holocene Southern Ocean surface temperature variability west of the Antarctic Peninsula. Nature 470 (7333), 250-254.
Sikes, E.L., Howard, W.R., Neil, H.L., Volkman, J.K., 2002. Glacial-interglacial sea surface temperature changes across the subtropical front east of New Zealand based on alkenone unsaturation ratios and foraminiferal assemblages. Paleoceanography 17 (2), doi:10.1029/2001PA000640.
Sluijs, A., Schouten, S., Pagani, M., Woltering, M., Brinkhuis, H., Sinninghe Damsté, J.S., Dickens, G.R., Huber, M., Reichart, G.-J., Stein, R., Matthiessen, J., Lourens, L.J., Pedentchouk, N., Backman, J., Moran, K., and the Expedition 302 Scientists, 2006. Subtropical Arctic Ocean temperatures during the Paleocene/Eocene thermal maximum. Nature 441, 610-613.

908 Spang, A., Hatzenpichler, R., Brochier-Armanet, C., Rattei, T., Tischler, P., Spieck, E., Streit,
909 W., Stahl, D.A., Wagner, M., Schleper, C., 2010. Distinct gene set in two different
910 lineages of ammonia-oxidizing archaea supports the phylum Thaumarchaeota.
911 Trends in Microbiology 18 (8), 331-340.
912 Turich, C., Schouten, S., Thunell, R.C., Varela, R., Astor, Y., Wakeham, S.G., 2013.
913 Comparison of TEX_{86} and temperature proxies in sinking particles in the Cariaco
914 Basin. Deep Sea Research Part I: Oceanographic Research Papers 78 (0), 115-133.
915 Van Camp, L., Nykjaer, L., Mittelstaedt, E., Schlittenhardt, P., 1991. Upwelling and
916 boundary circulation off Northwest Africa as depicted by infrared and visible
917 satellite observations. Progress in Oceanography 26 (4), 357-402.
918 Wakeham, S.G., Lewis, C.M., Hopmans, E.C., Schouten, S., Sinninghe Damsté, J.S., 2003.
919 Archaea mediate anaerobic oxidation of methane in deep euxinic waters of the
920 Black Sea. Geochimica et Cosmochimica Acta 67 (7), 1359-1374.
921 Wuchter, C., Schouten, S., Wakeham, S.G., Sinninghe Damsté, J.S., 2006. Archaeal
922 tetraether membrane lipid fluxes in the northeastern Pacific and the Arabian Sea:
923 Implications for the TEX_{86} paleothermometry. Paleoceanography 21, PA4208.
924 Xie, S., Liu, X.-L., Schubotz, F., Wakeham, S.G., Hinrichs, K.-U., 2014. Distribution of
925 glycerol ether lipids in the oxygen minimum zone of the Eastern Tropical North
926 Pacific Ocean. Organic Geochemistry 71 (0), 60-71.
927 Yamamoto, M., Shimamoto, A., Fukuhara, T., Tanaka, Y., Ishizaka, J., 2012. Glycerol dialkyl
928 glycerol tetraethers and TEX_{86} index in sinking particles in the western North
929 Pacific. Organic Geochemistry 53 (0), 52-62.
930 Zenk, W., Klein, B., Schroder, M., 1991. Cape Verde Frontal Zone. Deep Sea Research Part
931 A. Oceanographic Research Papers 38, Supplement 1 (0), S505-S530.
932
933
934

Table 1

Locations, deployment depths and dates of the CBeu sediment trap during the four deployment periods. Each trap was equipped with 20 cups (40 cups for CBeu-4o); traps were programmed to collect sinking particles during 20 (40) periods of equal duration during the deployment periods ("sampling interval"). Exact dates can be found along with proxy data on www.pangaea.de (doi:10.1594/PANGAEA.835471)

	Latitude (°N)	Longitude (°W)	Depth (m)	Deployment period start	Deployment period end	Sampling interval (d)
CBeu- 1o	20°45'	18°42'	1296	15 Jun 2003	05 Apr 2004	15.5
CBeu- 2o	20°45'	18°42'	1296	18 Apr 2004	20 Jul 2005	22 (1x), 23
CBeu- 3o	20°45.5'	18°41.9'	1277	25 Jul 2005	28 Sep 2006	21.5
CBeu- 4o	20°44.9'	18°42'	1256	28 Oct 2006	23 Mar 2007	7.5

Table 2

Details of SPM sampling from surface waters using the ships' seawater inlets: Sampling date, location, volume of seawater filtered, SST recorded by the ships' thermometers during sampling (average value), and $U^{K'}_{37}$ and TEX_{86}.

Filter No.	Date (mm/dd/yyyy)	Latitude [N] Start	Stop	Longitude [W] Start	Stop	Volume [L]	SST [°C] Ships' thermometer	$U^{K'}_{37}$	TEX_{86}
1	3/16/2009	12°26.057'	12°26.057'	18°00.294'	18°00.29 4'	136	19	0.47	0.56
2	3/17/2009	13°29.805'	13°26.660'	18°27.757'	18°22.95 2'	100	19	0.6	0.54
3	3/18/2009	13°51.731'	13°51.900'	17°25.774'	17°22.46 5'	154	19	0.46	0.53
4	3/18/2009	15°30.081'	15°24.054'	17°58.366'	17°54.24 0'	142	19	0.49	-
5	3/19/2009	15°23.181'	15°27.394'	17°12.248'	17°10.13 0'	45	19	0.31	0.53
6	3/21/2009	15°41.307'	15°44.595'	17°16.183'	17°15.50 4'	140	19.8	0.5	0.53
7	3/21/2009	15°40.848'	15°40.848'	17°16.017'	17°16.05 4'	144	19.8	0.61	-
8	3/21/2009	15°20.481'	15°16.271'	17°04.992'	17°03.02 2'	83	19.2	0.49	0.53
9	3/22/2009	15°28.289'	15°33.321'	16°49.559'	16°46.37 0'	94	18.6	0.54	0.56
10	3/22/2009	15°28.289'	15°52.662'	16°40.504'	16°44.39 3'	112	18.35	0.43	0.49
11	3/23/2009	17°03.307'	17°17.056'	16°43.739'	16°45.56 0'	147	18.65	0.45	0.51
12	3/24/2009	19°16.16'	19°14.863'	17°30.780'	17°34.301 '	136	18.3	0.47	0.49
13	3/25/2009	19°18.147'	19°16.002'	19°07.157'	19°02.74 7'	81	19.9	0.57	0.59
14	3/26/2009	19°37.029'	19°28.873'	16°58.359'	17°04.68 9'	164	17.15	0.5	0.49
15	3/26/2009	19°32.853'	19°34.845'	17°15.453'	17°16.98 2'	100	18.55	0.47	0.49
16	3/26/2009	19°57.365'	20°00.694'	17°21.159'	17°24.967'	79	17.9	0.42	0.5
17	3/27/2009	20°05.680'	20°05.677'	18°49.651'	18°49.65 0'	150	20.7	0.63	0.52
18	3/28/2009	21°19.996'	21°19.997	18°50.509'	18°50.508 '	133	19.7	0.51	0.53
19	3/29/2009	20°46.125'	20°46.125'	18°41.767'	18°41.76 6	115	20.5	0.66	0.5
20	3/30/2009	20°34.718'	20°34.699'	17°58.803'	17°58.80 3'	151	18.6	0.49	0.49
21	4/1/2009	21°00.006'	21°00.006'	19°50.003'	19°50.006 '	166	20.3	0.45	0.53
22	4/1/2009	21°15.606'	21°15.605'	20°46.403'	20°46.406 '	156	20.8	0.64	0.59
23	4/3/2009	21°37.623'	21°56.943'	20°10.789'	19°49.481 '	300	20.9	0.63	0.59
24	4/4/2009	24°13.839'	24°13.837'	17°17.366'	17°17.368 '	233	19.75	0.64	-
25	4/6/2009	26°26.400'	26°22.250'	14°54.787'	14°57.710 '	279	19.1	0.53	0.54
26	4/7/2009	27°32.233'	27°32.226'	13°44.127'	13°49.019 '	200	18.55	0.5	0.53
27	2/25/2010	23°58.06'	23°50.25'	18°36.77'	18°43.30 '	92	22.2	0.82	0.60
28	2/26/2010	20°15.15'	21°50.21'	20°15.19'	20°22.88'	94	22.2	0.85	-
29	2/26/2010	21°16.68'	21°16.68'	20°50.78'	20°50.77 '	77	23.3	0.85	0.59
30	2/27/2010	21°15.66'	21°15.66'	20°51.06'	20°51.06 '	93	23.3	0.86	0.60
31	2/28/2010	20°44.51'	20°44.51'	18°44.38'	18°44.39 '	74	21.9	0.80	0.5871
32	3/1/2010	20°35.66'	20°37.05'	18°02.16'	18°12.22'	51	21.3	0.55	0.57
33	3/2/2010	19°09.99'	19°09.99'	21°00.03'	21°00.03'	108	22.9	0.80	0.53

34	3/3/2010	20°26.42’	20°38.20’	19°09.04’	18°15.20’	93	21.4	0.72	0.58
35	3/4/2010	20°39.98’	20°39.98’	18°30.00’	18°30.00’	52	21.6	0.75	0.55
36	3/4/2010	20°35.37’	20°35.37’	17°59.7’	17°59.70’	60	21.0	0.77	0.54
37	3/5/2010	20°30.97’	20°35.00’	17°47.88’	17°59.99’	95	21.0	0.46	0.47

946

Figure captions

Figure 1

Oceanographic setting of the deep-ocean sediment trap mooring site CB_{eu} within the Cape Blanc filament, Mauritania. The filament dissolves into eddies further offshore. The Cape Verde Frontal Zone (CVFZ) separates the North and South Atlantic Central Water subsurface water masses (Zenk et al., 1991). Ocean colour map from MODIS in the insert upper left is shown for January 2005, indicating high chlorophyll concentrations and the extension of the Cape Blanc filament in winter (arrow).

CC=Canary Current, MC=Mauritanian Current; NEC=North Equatorial Current.

Figure 2

Correlation of biomarker proxy data of suspended particulate matter (SPM; black symbols) and published calibration data sets (grey symbols) with sea surface temperature (SST) or measured in-situ temperature. Black symbols: $U^{K'}_{37}$ (a,c) and TEX_{86} (b,d) for samples SPM collected during MSM11-2 and POS396 from the ship's sea water inlet at approximately 5 m water depth plotted versus the sea surface temperature measured during collection. Grey symbols and black lines mark the calibration data sets and calibration regressions (a) from Conte et al. (2006) for $U^{K'}_{37}$ of SPM, (b) from Schouten et al., (2013b) for TEX_{86} of SPM from <100 m (note that here the TEX_{86} data are correlated with measured in-situ temperature), (c) from Conte et al., (2006) for $U^{K'}_{37}$ of core-top sediments versus annual mean SST, and (d) the logarithmic form for samples >15°C from Kim et al. (2010) for TEX_{86} of surface sediments versus annual mean SST.

Figure 3

Records of (a) SST at 20.45°N, 18.41°W near the mooring site of CBeu obtained by Advanced Very High Resoltuion Radiometer (AVHRR) and averaged for the trap sampling periods, (b) $U^{K'}_{37}$, (c) alkenone flux (d) TEX_{86} (grey line: record obtained at NIOZ, black line: record obtained in Bremen (see text for details); triangles indicate duplicate measurements of trap series CBeu-2 to -4 made at NIOZ), (e) GDGT flux, and (f) mass fluxes recorded at CBeu.

Figure 4

Correlations of mass flux with TOC (a) and opal flux (b), and of TOC (c, e), carbonate (d) and opal flux (f) with lipid fluxes for trap series CBeu-2 to -4 and coefficients of determination. Note that GDGT fluxes are given in arbitrary units, as the concentrations of GDGTs were not determined relative to a standard (see text for details). For better comparability, the alkenone flux is also only shown for trap series CBeu-2 to -4. Symbols refer to CBeu-1o (open circles), CBeu-2o (filled triagles), CBeu-3o (crosses), and CBeu-4o (filled squares).

Figure 5

Sea surface temperature estimates (black lines) based on (a) $U^{K'}_{37}$ using the SPM calibration from Conte et al. (2006), (b) $U^{K'}_{37}$ using the core-top sediment calibration from Conte et al. (2006), (c) TEX_{86} using the SPM calibration proposed by Schouten et al., (2013b), and (d) TEX_{86} using the logarithmic calibration for sediments from Kim et al., 2010. The grey lines are the AVHRR SST data. Note the different vertical axis scales.

.

Figure 1

Click here to download high resolution image

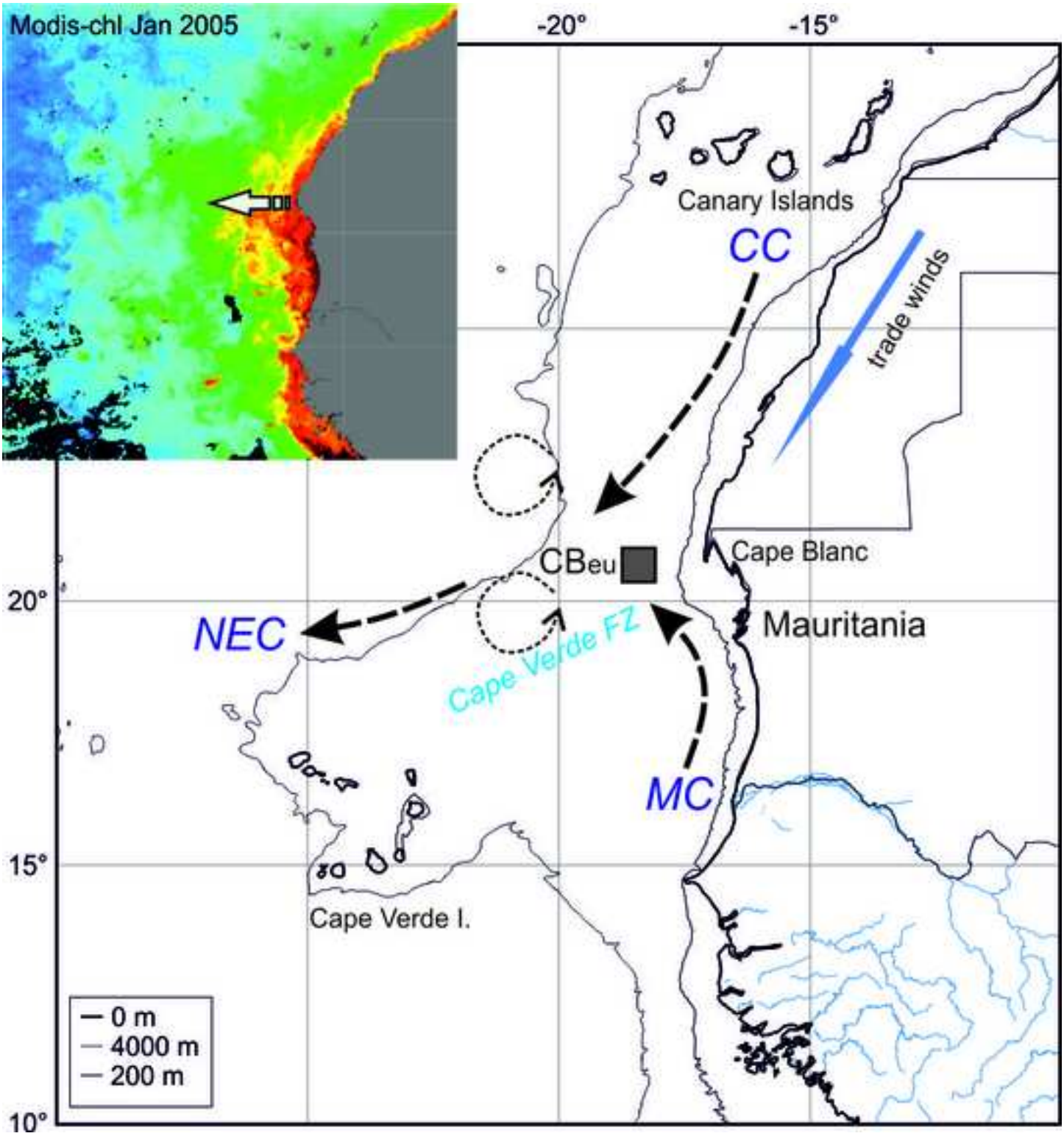

Figure 2

Click here to download Figure: Figure 2.pdf

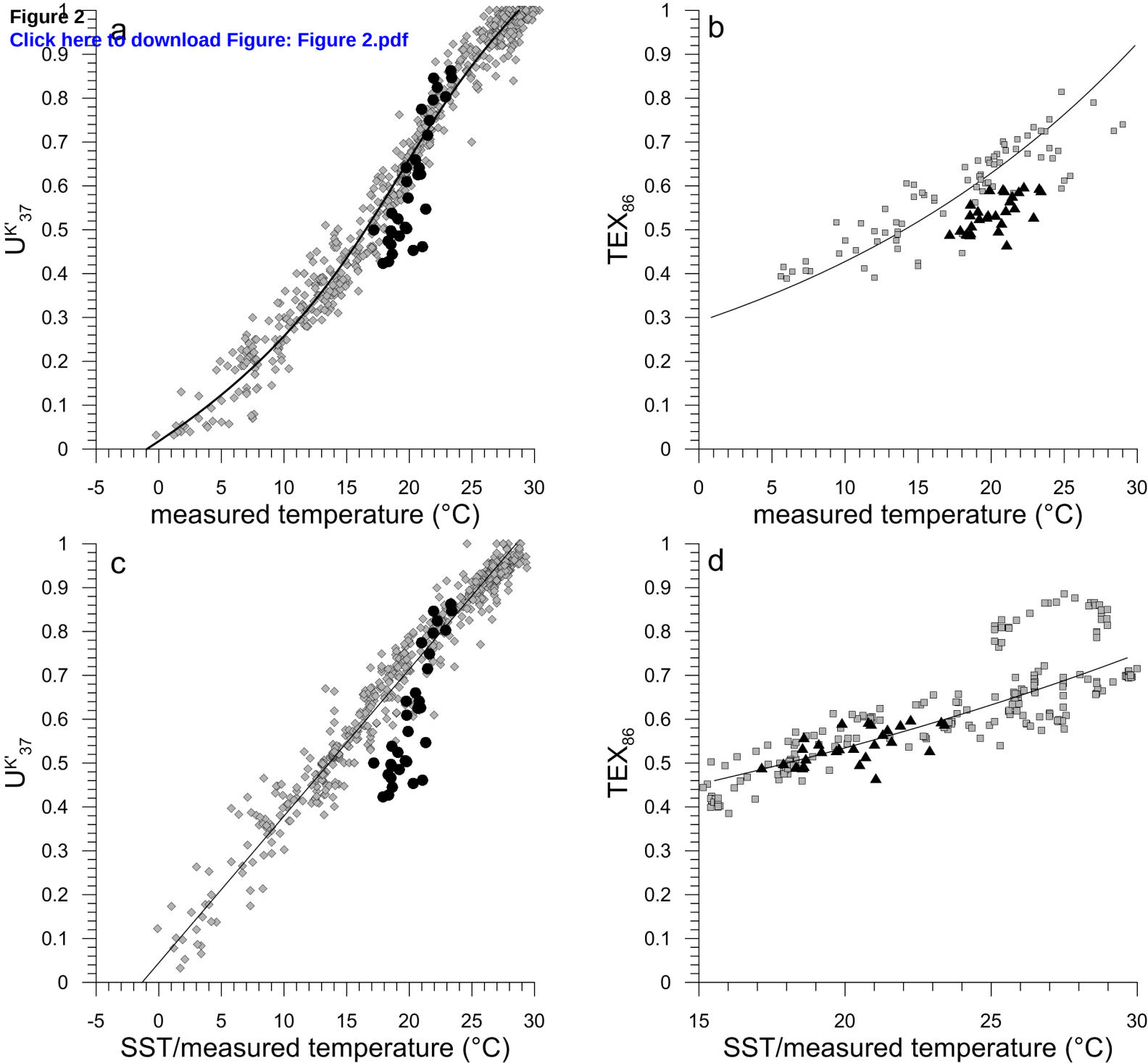

Figure 3

Click here to download Figure: Figure 3.pdf

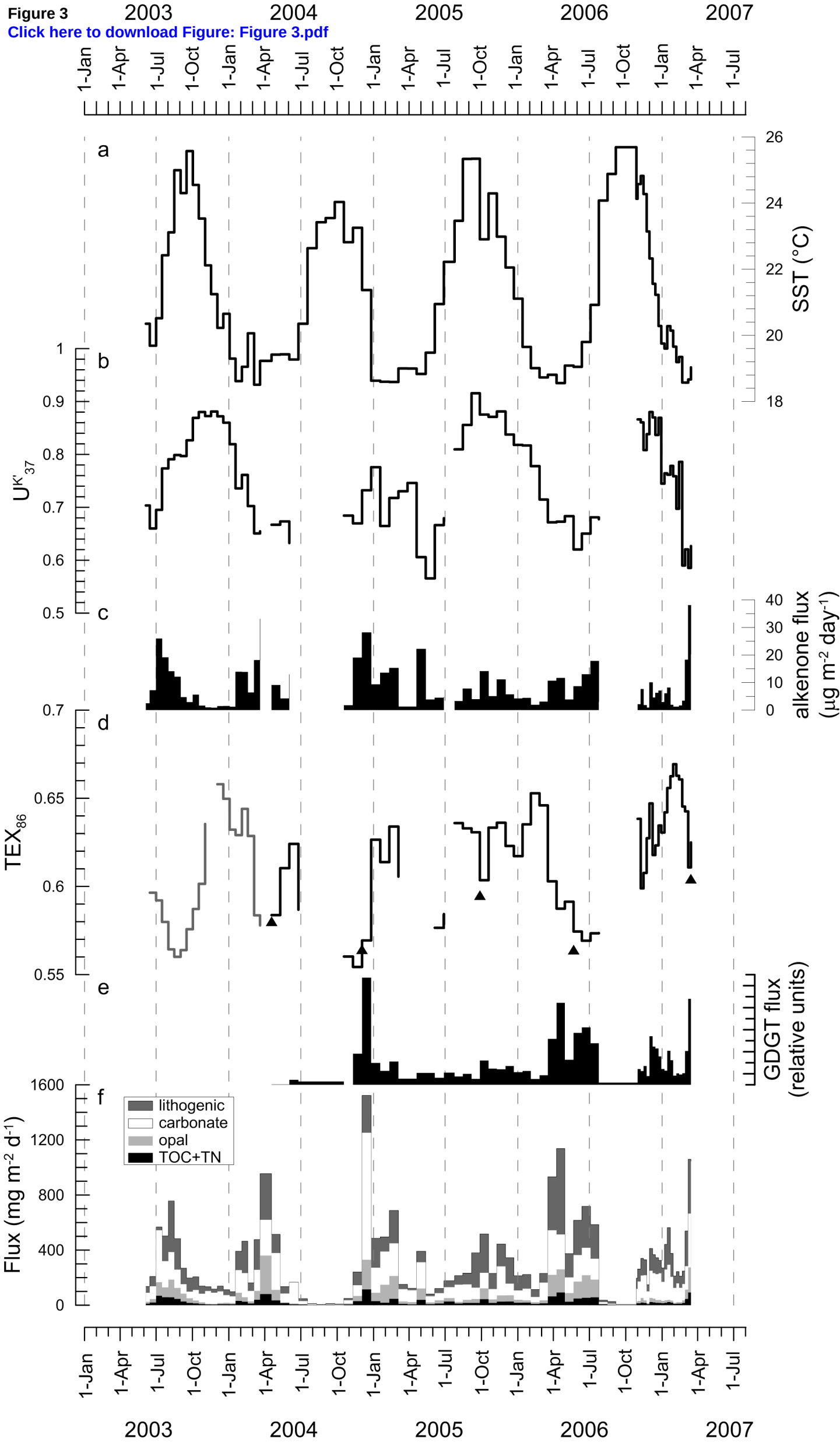

Figure 4

Click here to download Figure: Figure 4.pdf

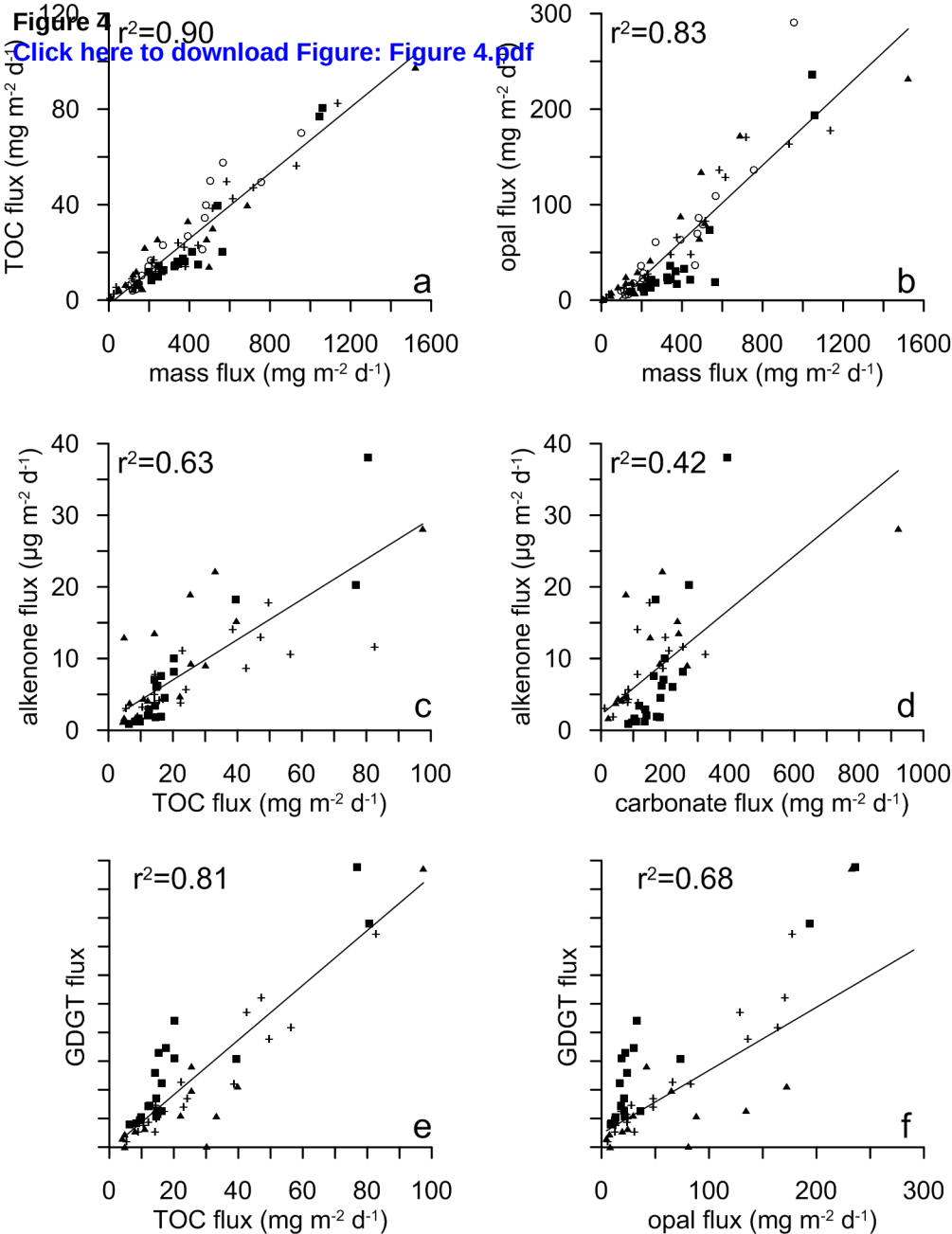

Figure 5